

## Active Chiral Processes in Thin Films

S. Fürthauer,<sup>1,2</sup> M. Stempel,<sup>1,2</sup> S. W. Grill,<sup>1,2</sup> and F. Jülicher<sup>1</sup><sup>1</sup>Max Planck Institute for the Physics of Complex Systems, Nöthnitzer Straße 38, 01187 Dresden, Germany<sup>2</sup>Max Planck Institute of Molecular Cell Biology and Genetics, Pfotenhauerstraße 108, 01307 Dresden, Germany

(Received 12 November 2011; revised manuscript received 12 October 2012; published 23 January 2013)

We develop a generic description of thin active films that captures key features of flow and rotation patterns emerging from the activity of chiral motors which introduce torque dipoles. We highlight the role of the spin rotation field and show that fluid flows can occur in two ways: by coupling of the spin rotation rate to the velocity field via a surface or by spatial gradients of the spin rotation rate. We discuss our results in the context of patches of bacteria on solid surfaces and groups of rotating cilia. Our theory could apply to active chiral processes in the cell cytoskeleton and in epithelia.

DOI: [10.1103/PhysRevLett.110.048103](https://doi.org/10.1103/PhysRevLett.110.048103)

PACS numbers: 87.18.Hf, 47.15.gm, 87.15.B-, 87.85.gf

The building blocks of biological systems are chiral molecules such as proteins and DNA. The emergent collective behaviors of these molecular components give rise to active dynamic processes in cells and tissues which reflect these molecular chiralities. A key example is the breaking of left-right symmetry in organisms with a well-defined handedness during development [1–4]. In vertebrate animals, it has been shown that the rotating beat of cilia, which drives chiral hydrodynamic flows, is at the basis of left-right symmetry breaking [5–8] (i.e., the heart is on the left side in humans).

Many pattern forming events in the cytoskeleton are also governed by active chiral processes. The cytoskeleton is a gel-like network of elastic chiral filaments and other components such as motor proteins. The interactions of motors and filaments drive movements and intracellular flows [9,10], which can have chiral asymmetries [11–14]. Active chiral processes have been observed in the *Xenopus* cell cortex [11] and crawling neurites [15]. Moreover, chiral movements in the *C. elegans* cell cortex have been suggested to be involved in the left-right symmetry breaking [16].

Further examples are rotating motors on a surface [17–19] and carpets of beating cilia used for fluid transport along surfaces [20,21]. Many microorganisms possess carpets of cilia on their outer surface, which are used for self-propulsion. Various beating patterns of cilia exist, which in general are chiral and often exhibit rotating movements resulting in helical trajectories of microswimmers [21]. The interaction of microswimmers with surfaces can lead to interesting effects [22]. Recently, flagellated *E. coli* bacteria [see Fig. 1(a)] close to a solid surface were reported to generate large scale chiral flow patterns [23].

The cell cytoskeleton and suspensions of active swimmers have been described as active fluids and gels and studied in the framework of hydrodynamic theories [24–29]. Such approaches are based on liquid crystal hydrodynamics [30–35] driven out of equilibrium by internal active processes. It has been shown that stresses

generated by active processes can give rise to a rich variety of dynamic patterns and flows [10,36–41]. Similar approaches have also been used for the study of granular systems [42,43]. Recently, we proposed a systematic extension of the theory of active gels to active chiral fluids [44], in which active contributions to the antisymmetric stress and active angular momentum fluxes are generated by microscopic torque dipoles which arise in situations where interacting objects counterrotate. Examples of torque dipoles are the counterrotation of cell body and flagella of swimming bacteria, see Fig. 1(a), helical actin filaments interacting via clusters of myosin motors; see Fig. 1(b). Thus, in general suspensions of chiral swimmers as well as the cell cytoskeleton can be considered to be active chiral fluids.

Many of the most striking active chiral effects, including the biological examples mentioned above, have been observed at interfaces and close to boundaries [2,3,45]. It

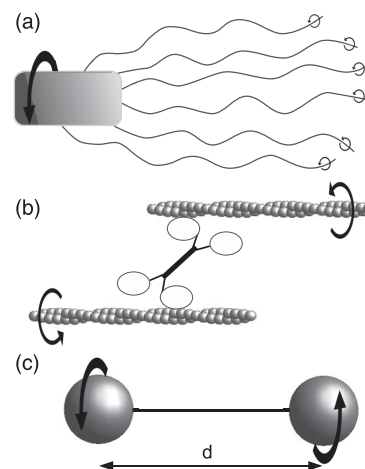


FIG. 1. Examples of active torque dipoles. Black arrows indicate the torques. (a) A swimming bacterium with rotating flagella. (b) Cytoskeletal torque dipole consisting of two actin filaments and myosin motors. (c) Idealized chiral motor consisting of two counterrotating spheres at distance  $d$ .

is the aim of the present work to derive a generic theory for active chiral films. To capture the effect of torque dipoles in complex fluids, we need to explicitly consider a local spin degree of freedom [44]. We show that in active chiral systems the intrinsic or “spin” rotation rate can be different from the vorticity of the flow field even at steady state. This is different from conventional soft matter [32,33,35]. We show furthermore that the coupling between the spin rotation rate and momentum fluxes can give rise to large scale flows. We discuss these behaviors in the context of the fluid flows generated by simple experimental systems such as beating cilia and bacteria adhering to a surface and close with a discussion of other systems where our theory is relevant such as the cell cortex.

We start by briefly reviewing the bulk properties of an active chiral fluid [44] in order to introduce the relevant concepts. Linear momentum and angular momentum conservation can be expressed as

$$\partial_t(\rho \mathbf{v}_\alpha) = \partial_\beta \sigma_{\alpha\beta}^{\text{tot}} + \mathbf{f}_\alpha^{\text{ext}}, \quad (1)$$

$$\partial_t l_{\alpha\beta}^{\text{tot}} = \partial_\gamma M_{\alpha\beta\gamma}^{\text{tot}} + \tau_{\alpha\beta}^{\text{ext}} + r_\alpha f_\beta^{\text{ext}} - r_\beta f_\alpha^{\text{ext}}, \quad (2)$$

where  $\rho$  denotes mass density,  $\mathbf{v}$  is the center of mass velocity and a summation convention is implied. Here,  $\rho \mathbf{v}$  is the momentum density. The density of angular momentum  $l_{\alpha\beta}^{\text{tot}}$  is described by an antisymmetric second rank tensor. Externally applied force and torque densities are denoted by  $\mathbf{f}^{\text{ext}}$  and  $\tau_{\alpha\beta}^{\text{ext}}$ , respectively,  $\mathbf{r}$  is a position vector,  $\sigma_{\alpha\beta}^{\text{tot}}$  is the total stress and  $M_{\alpha\beta\gamma}^{\text{tot}}$  is the total angular momentum flux. The total stress  $\sigma_{\alpha\beta}^{\text{tot}} = -P\delta_{\alpha\beta} + \sigma_{\alpha\beta}^s + \sigma_{\alpha\beta}^a$  describes momentum fluxes and can be decomposed in the isotropic pressure  $P$ , the symmetric traceless stress  $\sigma_{\alpha\beta}^s$  and the antisymmetric stress  $\sigma_{\alpha\beta}^a$ . The total angular momentum density consists of an orbital part  $\rho(r_\alpha \mathbf{v}_\beta - r_\beta \mathbf{v}_\alpha)$  and a spin angular momentum density  $l_{\alpha\beta} = l_{\alpha\beta}^{\text{tot}} - \rho(r_\alpha \mathbf{v}_\beta - r_\beta \mathbf{v}_\alpha)$ , see Refs. [30,31,35,45], which is usually ignored but plays a central role in active chiral systems. Similarly, the total angular momentum flux  $M_{\alpha\beta\gamma}^{\text{tot}} = M_{\alpha\beta\gamma} + (r_\alpha \sigma_{\beta\gamma}^{\text{tot}} - r_\beta \sigma_{\alpha\gamma}^{\text{tot}})$  is the sum of fluxes  $M_{\alpha\beta\gamma}$  and  $r_\alpha \sigma_{\beta\gamma}^{\text{tot}} - r_\beta \sigma_{\alpha\gamma}^{\text{tot}}$  of spin and orbital angular momentum, respectively. Note that the spin angular momentum density  $l_{\alpha\beta}$  and the spin angular momentum flux  $M_{\alpha\beta\gamma}$  do not depend on the choice of the coordinate system. We define an effective rate of spin rotation  $\Omega_{\alpha\beta}$  of local volume elements via  $l_{\alpha\beta} = I_{\alpha\beta\gamma\delta} \Omega_{\gamma\delta}$ , where  $I_{\alpha\beta\gamma\delta}$  is the moment of inertia tensor per unit volume [35]. The spin angular momentum then obeys

$$\partial_t l_{\alpha\beta} = -2\sigma_{\alpha\beta}^a + \partial_\gamma M_{\alpha\beta\gamma} + \tau_{\alpha\beta}^{\text{ext}}, \quad (3)$$

which shows that spin and orbital angular momentum are not individually conserved but can be exchanged through antisymmetric stress.

We discuss the effects of an active chiral process by considering a torque dipole  $\tau_{\alpha\beta}(\mathbf{r})$  in a fluid, located at

$\mathbf{r} = 0$ , see Fig. 1(c). This torque dipole is built from two torque monopoles  $\pm q\epsilon_{\alpha\beta\gamma} p_\gamma$ , of strength  $q$  separated by a small distance  $d$  in the direction of the torque axis given by the unit vector  $\mathbf{p}$ :

$$\begin{aligned} \tau_{\alpha\beta} &= q\epsilon_{\alpha\beta\gamma} p_\gamma \left[ \delta\left(\mathbf{r} - \frac{d}{2}\mathbf{p}\right) - \delta\left(\mathbf{r} + \frac{d}{2}\mathbf{p}\right) \right] \\ &\simeq -qd\epsilon_{\alpha\beta\nu} p_\nu p_\gamma \partial_\gamma \delta(\mathbf{r}). \end{aligned} \quad (4)$$

Note that  $\tau_{\alpha\beta}$  is invariant under the transformation  $\mathbf{p} \rightarrow -\mathbf{p}$ , which implies a nematic character.

From Eq. (3) the torque dipole  $\tau_{\alpha\beta}$  can be interpreted as an active contribution  $M_{\alpha\beta\gamma}^{\text{act}} = -qd\epsilon_{\alpha\beta\delta} p_\delta p_\gamma \delta(\mathbf{r})$  to the spin angular momentum flux, which obeys  $\partial_\gamma M_{\alpha\beta\gamma}^{\text{act}} = \tau_{\alpha\beta}$ . In a suspension of many identical torque dipoles at positions  $\mathbf{r}^{(i)}$  and with orientations  $\mathbf{p}^{(i)}$ , the active angular momentum fluxes are

$$\begin{aligned} M_{\alpha\beta\gamma}^{\text{act}} &= -qd \sum_i \epsilon_{\alpha\beta\delta} p_\delta^{(i)} p_\gamma^{(i)} \delta(\mathbf{r} - \mathbf{r}^{(i)}) \\ &\simeq \zeta \epsilon_{\alpha\beta\delta} p_\delta p_\gamma + \zeta' \epsilon_{\alpha\beta\gamma}, \end{aligned} \quad (5)$$

where  $\zeta = -Sqdn$  and  $\zeta' = (S-1)qdn/3$  describe the strength of a nematic and an isotropic active contribution to  $M_{\alpha\beta\gamma}$ , respectively, and  $n$  is the dipole density. Here and below,  $\mathbf{p}$ , with  $\mathbf{p}^2 = 1$ , denotes a coarse-grained nematic director and  $S$  is a nematic order parameter obeying  $S(p_\alpha p_\beta - (1/3)\delta_{\alpha\beta}) = \langle p_\alpha^{(i)} p_\beta^{(i)} \rangle - (1/3)\delta_{\alpha\beta}$ , where the average is taken over a volume element [33].

The constitutive equation for the spin angular momentum flux then has the form

$$M_{\alpha\beta\gamma} = \kappa \partial_\gamma \Omega_{\alpha\beta} + \zeta \epsilon_{\alpha\beta\delta} p_\delta p_\gamma + \zeta' \epsilon_{\alpha\beta\gamma}. \quad (6)$$

Here, the term proportional to the phenomenological coefficient  $\kappa$  describes passive dissipative processes [35,44]. For simplicity, we ignore other passive couplings and neglect inertial terms.

We complement Eq. (6) by the constitutive equations of a passive incompressible fluid:

$$\sigma_{\alpha\beta}^s = 2\eta \tilde{u}_{\alpha\beta} + \frac{\nu_1}{2} \left( p_\alpha h_\beta + p_\beta h_\alpha - \frac{2}{3} \delta_{\alpha\beta} h_\gamma p_\gamma \right), \quad (7)$$

$$\sigma_{\alpha\beta}^a = 2\eta' (\Omega_{\alpha\beta} - \omega_{\alpha\beta}) + \frac{\nu_2}{2} (p_\alpha h_\beta - p_\beta h_\alpha), \quad (8)$$

where,  $\eta$  is the shear viscosity and  $\eta'$  is a rotational viscosity [44]. Here,  $\tilde{u}_{\alpha\beta}$  is the traceless part of the strain rate  $u_{\alpha\beta} = (\partial_\alpha \mathbf{v}_\beta + \partial_\beta \mathbf{v}_\alpha)/2$ ,  $\omega_{\alpha\beta} = (\partial_\alpha \mathbf{v}_\beta - \partial_\beta \mathbf{v}_\alpha)/2$  is the vorticity and  $\mathbf{h} = -\delta F/\delta \mathbf{p}$  is the distortion field conjugated to  $\mathbf{p}$ , where  $F$  is the distortion free energy. Other additional coupling terms known to exist in liquid crystals have been neglected for simplicity. In the present Letter, the only active processes we consider are the ones stemming from the torque dipole Eq. (4). We thus ignore possible active contributions to the symmetric part of the stress tensor. The pressure  $P$  plays the role of a Lagrange

multiplier and is imposed by the incompressibility condition  $\partial_\gamma v_\gamma = 0$ .

The orientation vector  $\mathbf{p}$  changes due to flow alignment and convection. It obeys the dynamic equation

$$\partial_t p_\alpha + v_\beta \partial_\beta p_\alpha + \Omega_{\alpha\beta} p_\beta = \frac{1}{\gamma} h_\alpha - \nu_1 u_{\alpha\beta} p_\beta - \nu_2 (\Omega_{\alpha\beta} - \omega_{\alpha\beta}) p_\beta. \quad (9)$$

Together, Eqs. (6)–(9) are the bulk equations of motion of the active chiral fluid and provide the basis for our discussion of thin active chiral films.

We now study the stresses and flows generated by active chiral processes in a thin fluid film of constant height  $h$  on a solid substrate in the  $xy$  plane; see Fig. 2. Note that the film can be asymmetric with respect to  $z \rightarrow h - z$  if the two surfaces at  $z = 0$  and  $z = h$  differ. For simplicity, we will consider films in which the polarization field  $\mathbf{p}$  remains constant over the thickness  $h$ .

To obtain equations of motion in the thin film, we integrate the force balance Eq. (1) with  $\mathbf{f}^{\text{ext}} = 0$  over the film thickness and obtain

$$\frac{1}{h} \int_0^h dz \partial_\beta \sigma_{i\beta}^{\text{tot}} = \partial_j \bar{\sigma}_{ij}^{\text{tot}} + \frac{1}{h} \sigma_{iz}^{\text{tot}}|_0^h = 0, \quad (10)$$

where the bar denotes an average over the film height,  $\bar{\sigma}_{i\beta}^{\text{tot}} \equiv (1/h) \int_0^h dz \sigma_{i\beta}^{\text{tot}}$ , and  $\sigma_{iz}^{\text{tot}}|_0^h \equiv \sigma_{iz}^{\text{tot}}(z=h) - \sigma_{iz}^{\text{tot}}(z=0)$ , where  $i, j = x, y$ ; see Fig. 2. We express the shear stress at the film surfaces as resulting from friction forces

$$\frac{1}{h} \sigma_{iz}^{\text{tot}}|_0^h = -\xi_i \bar{v}_i + \xi_\Omega \bar{\Omega}_{iz}. \quad (11)$$

Friction due to relative motion and relative rotation with the substrate is described by the coefficients  $\xi_i$  and  $\xi_\Omega$ , respectively [46]. Note that although Eq. (11) explicitly contains spin rotation rates, it is not chiral since it is invariant towards the inversion of the coordinate system  $\mathbf{r} \rightarrow -\mathbf{r}$ . Note also that the term  $\xi_\Omega \bar{\Omega}_{iz}$  must vanish if the film is symmetric with respect to  $z \rightarrow h - z$ .

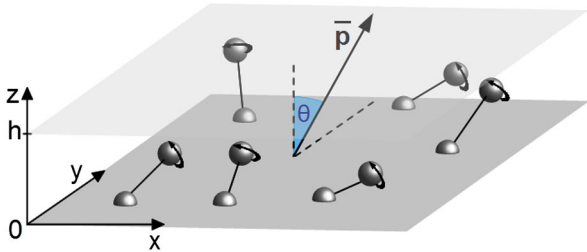


FIG. 2 (color online). Schematics of a thin fluid film of height  $h$  that contains chiral motors. Motors are torque dipoles that consist of counterrotating spheres [see Fig. 1(b)], one of which is attached to the surface. The other rotates as indicated by the arrows. The average motor direction is described by the vector  $\mathbf{p}$  which is tilted at an angle  $\theta$  in  $y$ -direction.

Similarly, integrating Eq. (3) over the film thickness for  $\tau_{\alpha\beta}^{\text{ext}} = 0$  we obtain

$$\partial_j \bar{M}_{\alpha\beta j} - 2\bar{\sigma}_{\alpha\beta}^a + \frac{1}{h} M_{\alpha\beta z}|_0^h = 0. \quad (12)$$

Similar to Eq. (11), we express the torque densities on the surfaces. We take into account friction forces due to local rotation described by the coefficient  $\xi_r$ . Furthermore, we consider surface torques generated by torque dipoles which are attached to the surface by one end, see Fig. 2, thereby creating active chiral surface effects. The torque densities at the surfaces then read

$$\frac{1}{h} M_{\alpha\beta z}|_0^h = -\xi_r \bar{\Omega}_{\alpha\beta} + \zeta_s \epsilon_{\alpha\beta\delta} p_z p_\delta + \zeta'_s \epsilon_{\alpha\beta z}. \quad (13)$$

Here, the effects of torque dipoles attached to the surfaces are described by the coefficients  $\zeta_s$  and  $\zeta'_s$ . While the friction term proportional to  $\xi_r$  in Eq. (13) is inversion symmetric, the two active terms are chiral and vanish in film symmetric with respect to  $z \rightarrow h - z$ .

We now compile the equations of motion of the active chiral films in the absence of external shear stresses and pressure gradients. In the presence of an external applied shear stress on the boundaries we have  $\bar{\sigma}_{iz} \approx \sigma_{iz}^{\text{ext}}$ . Thus, in the absence of external shear stresses,  $v_i|_0^h = -2h\eta'\bar{\Omega}_{iz}/(\eta + \eta') - (\nu_1 + \nu_2)hp_i h_z/2/(\eta + \eta') - (\nu_1 - \nu_2)hp_i h_z/2/(\eta + \eta')$ . Similarly,  $P^{\text{ext}} \approx \bar{\sigma}_{zz}^{\text{tot}}$  is the externally applied pressure and we find,  $\bar{P} - P^{\text{ext}} \approx -2\eta\partial_i \bar{v}_i + \nu_1 p_z h_z - \nu_1 h_\alpha p_\alpha/3$ . We finally obtain equations of motion for the flow and rotation field:

$$0 = \partial_j [(3\eta - \eta')\partial_i \bar{v}_j + (\eta + \eta')\partial_j \bar{v}_i] + 2\eta'\partial_j \bar{\Omega}_{ij} - \partial_i \nu_1 p_z h_z + \frac{\nu_1 + \nu_2}{2} \partial_j (p_i h_j) + \frac{\nu_1 - \nu_2}{2} \partial_j (p_j h_i) - \xi_i \bar{v}_i + \xi_\Omega \bar{\Omega}_{iz}, \quad (14)$$

$$0 = -(4\eta' + \xi_r)\bar{\Omega}_{xy} + 2\eta'(\partial_x \bar{v}_y - \partial_y \bar{v}_x) - \nu_2(p_x h_y - p_y h_x) + \kappa\partial_j^2 \bar{\Omega}_{xy} + \partial_j \zeta \epsilon_{xyz} p_z p_j + \zeta_s \epsilon_{xyz} p_z^2 + \zeta'_s \epsilon_{xyz}, \quad (15)$$

$$0 = -\left(\frac{4\eta\eta'}{\eta + \eta'} + \xi_r\right)\bar{\Omega}_{iz} + \kappa\partial_j^2 \bar{\Omega}_{iz} - \nu_2(p_i h_z - p_z h_i) + \frac{\eta'(\nu_1 + \nu_2)}{\eta + \eta'} p_i h_z + \frac{\eta'(\nu_1 - \nu_2)}{\eta + \eta'} p_i h_z + \partial_j \zeta \epsilon_{iz\delta} p_\delta p_j + \partial_j \zeta' \epsilon_{izj} + \zeta_s \epsilon_{iz\delta} p_\delta p_z. \quad (16)$$

We obtain the dynamic equation for  $\mathbf{p}$  by averaging Eq. (9) over the thin film,

$$\begin{aligned} \partial_i p_\alpha &= \frac{1}{\gamma} h_\alpha - \bar{v}_i \partial_i p_\alpha - (\nu_2 + 1) \bar{\Omega}_{\alpha\beta} p_\beta \\ &\quad - \frac{\nu_1 - \nu_2}{2} \left( \delta_{\alpha i} (\partial_i \bar{v}_\beta) + \frac{1}{h} \delta_{\alpha z} v_{\beta 0} \right) p_\beta \\ &\quad - \frac{\nu_1 + \nu_2}{2} \left( \delta_{\beta i} (\partial_i \bar{v}_\alpha) + \frac{1}{h} \delta_{\beta z} v_{\alpha 0} \right) p_\beta. \end{aligned} \quad (17)$$

Here, we used the thin film approximation  $\partial_i v_z \ll \partial_z v_i$ .

To illustrate the key features of our theory, we now consider a thin active film containing torque dipoles that are on average aligned along the constant vector  $\mathbf{p} = (\cos\phi \sin\theta, \sin\phi \sin\theta, \cos\theta)$ . Here, we have introduced the angle  $\theta$  describing the average tilt with respect to the surface normal vector and the angle  $\phi$ , which specifies the tilt direction with respect to the  $x$  axis. The field  $\mathbf{h}$  then becomes a Lagrange multiplier that enforces the constraint of constant  $\mathbf{p}$ . Moreover for simplicity, we consider the case  $\nu_1 = \nu_2 = 0$ .

We first consider a homogeneous distribution of motors in an infinite system, where all spatial derivatives vanish. In this case, Eq. (14) reads  $\bar{v}_i = (\xi_\Omega / \xi_i) \bar{\Omega}_{iz}$ . Using Eq. (16), we find

$$\bar{v}_i = \frac{\xi_\Omega \zeta_s}{\xi_i} \frac{\epsilon_{izj} p_j p_z}{\xi_r + 4\eta\eta' / (\eta + \eta')}. \quad (18)$$

A flow with a velocity  $|\bar{\mathbf{v}}| \propto \xi_\Omega \zeta_s \sin(2\theta)$  is generated by an active interaction of the torque dipoles with the surface. The flow direction is perpendicular to the direction of tilt with respect to the surface normal vector. From Eq. (15) the spin is  $\bar{\Omega}_{xy} = (\zeta_s \cos^2\theta + \zeta'_s) / (4\eta' + \xi_r)$  while the vorticity of the flow field vanishes,  $\bar{\omega}_{xy} = 0$ .

We next consider a circular patch of radius  $R$  that contains active motors with constant  $\mathbf{p}$ . This is described by position dependent coefficients  $\zeta_s(\mathbf{r}) = \zeta_s \Theta(R - |\mathbf{r}|)$  and similar expressions for  $\zeta'_s$ ,  $\zeta$  and  $\zeta'$ , where  $\Theta(r)$  is the Heaviside function. We numerically solve Eqs. (14)–(16) in a box of size  $L = 4R$  with periodic boundary conditions using Fourier transforms. The velocity field for a tilt angle  $\theta = 0$  is displayed in Fig. 3(a). The active patch generates a chiral flow field driven by the spin  $\bar{\Omega}_{xy}$ . The stream lines are concentric circles. The flow velocity is maximal at the edge of the patch and decays exponentially outside. As for the homogeneous case with  $\theta = 0$ , there is no net transport across the patch. If the motors are tilted with  $\theta \neq 0$  along the  $y$  axis, a net transport in  $x$  direction across the patch with velocity proportional to  $\sin(2\theta)$  appears in addition to the circular flow; see Fig. 3(b). This result is a linear superposition of the flows generated by the tilt and the circular flows generated at the boundary of the patch.

These examples illustrate that local spin rotations can generate fluid flows. This can occur in two ways. (a) The spin rotation rate couples to the velocity field via the boundaries. This mechanism can generate large scale flows and net transport; see Eq. (18). (b) Flows are generated orthogonal to gradients of the spin rotation rate. These flows circulate around patches of rotating motors; see

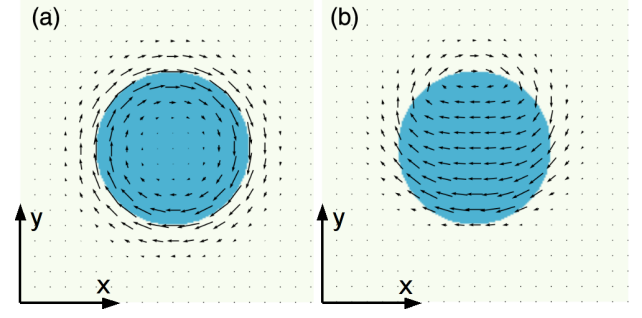


FIG. 3 (color online). Flow fields (vectors) generated by a circular patch of chiral motors (blue). (a) Average motor axis  $\mathbf{p}$  is perpendicular to the surface, i.e.,  $\theta = 0$ . (b) Average motor axis  $\mathbf{p}$  tilted at angle  $\theta = \pi/4$  in the  $y$  direction. Flow fields were determined numerically in a square box of size  $L$  with periodic boundary conditions. Parameter values are  $\eta' = \eta = h^2 \kappa = h^2 \xi_t = -h \xi_\Omega = \xi_r$ ,  $\zeta = -h \zeta_s = 10 \zeta' = -10 h \zeta'_s$ ,  $L = 20h$ .

Fig. 3. In all cases the spin rotation rate  $\bar{\Omega}_{xy}$  differs from the vorticity of the fluid flow  $\bar{\omega}_{xy}$ , even in steady state.

We now discuss our theory in the context of two biological examples of active chiral films: (i) *E. coli* bacteria placed on a solid agar surface were shown to generate chiral fluid flows [23]; (ii) rotating primary cilia produce flows that break left-right symmetry in developing organisms, as observed, e.g., in mouse [5–7] and zebrafish [47] embryos. In system (i), the bacterial flagella typically point away from the surface, while they may orient in all directions in the  $xy$  plane. Thus, the local average of flagella orientations characterized by  $\mathbf{p}$  points in the  $z$  direction. In system (ii), the average direction of cilia  $\mathbf{p}$  is kept constant by the anchoring of the cilia in tissue surface. Thus, for both examples, our assumption of constant  $\mathbf{p}$  applies.

In system (i), circular flow patterns are observed near the boundaries of bacterial patches, similar to the flows shown in Fig. 3(a). In system (ii), flows along the surface in the direction orthogonal to the tilt-direction of cilia are generated [6–8], similar to the flow shown in Fig. 3(b). According to Eq. (18), the velocity of the net flow is maximal for tilt angles of  $\theta = 45^\circ$ . Interestingly, reported tilt angles of cilia vary between  $30^\circ$  and  $50^\circ$  [48], which is close to the angle of maximum transport velocity in our theory.

We have developed a coarse grained description of flow patterns generated in active chiral films. Our theory highlights the role of the spin rotation field  $\Omega_{\alpha\beta}$  for active chiral processes. We show that unlike in inversion symmetric and passive chiral systems, where  $\Omega_{\alpha\beta} = \omega_{\alpha\beta}$  on long time and length scales [35], in active chiral systems  $\Omega \neq \omega$  even in steady state. We demonstrate that patterns of spin rotation can drive flows via coupling with the boundaries and gradients of spin rotation rate, as exemplified in beating cilia and bacterial patches, respectively.

Active chiral processes play an important role in biological pattern formation. Our theory is motivated in particular by chiral processes observed in the cell cortex



[11,15,16], which is a thin film of an active gel. Chiral flows of the cytoskeleton have been suggested to play a role in the formation of chiral asymmetric structures in cells and tissues [16]. On larger scales, two dimensional tissues called epithelia are also examples of active chiral films. Epithelia are active systems due to cell division, cell locomotion, and cell death and cell polarity plays the role of the direction  $\mathbf{p}$  of our theory. Chiral patterns have been shown to form in epithelia, such as the scalp hair whorl on human heads [49]. Our generic theory highlights the importance of chiral surface processes in active systems, which we expect to play a key role in the formation of chiral patterns in the cytoskeleton and in tissues.

S. Fürthauer and M. Strepel contributed equally to this work.

- 
- [1] L. Wolpert, *Principles of Development* (Oxford University Press, Oxford, 1998).
- [2] C.L. Henley, [arXiv:0811.0055v2](https://arxiv.org/abs/0811.0055v2).
- [3] C.L. Henley, *J. Stat. Phys.* **148**, 740 (2012).
- [4] L.N. Vandenberg and L. Levin, *Semin. Cell Dev. Biol.* **20**, 456 (2009).
- [5] S. Nonaka, Y. Tanaka, Y. Okada, S. Takeda, A. Harada, Y. Kanai, M. Kido, and N. Hirokawa, *Cell* **95**, 829 (1998).
- [6] S. Nonaka, S. Yoshida, D. Watanabe, S. Ikeuchi, T. Goto, W.F. Marshall, and H. Hamada, *PLoS Biol.* **3**, e268 (2005).
- [7] J. Buceta, M. Ibañes, D. Rasskin-Gutman, Y. Okada, N. Hirokawa, and J.C. Izpisua-Belmonte, *Biophys. J.* **89**, 2199 (2005).
- [8] D.J. Smith, J.R. Blake, and E.A. Gaffney, *J. R. Soc. Interface* **5**, 567 (2008).
- [9] J.W. van de Meent, I. Tuval, and R.E. Goldstein, *Phys. Rev. Lett.* **101**, 178102 (2008).
- [10] M. Mayer, M. Depken, J.S. Bois, F. Jülicher, and S.W. Grill, *Nature (London)* **467**, 617 (2010).
- [11] M. Danilchik, E.E. Brown, and K. Riegert, *Development (Cambridge, UK)* **133**, 4517 (2006).
- [12] I. Sase, H. Miyati, S. Ishiwata, and K. Kinoshita, Jr., *Proc. Natl. Acad. Sci. U.S.A.* **94**, 5646 (1997).
- [13] A. Hilfinger and F. Jülicher, *Phys. Biol.* **5**, 016003 (2008).
- [14] A. Vilfan, *Biophys. J.* **97**, 1130 (2009).
- [15] A. Tamada, S. Kawase, F. Murakami, and H. Kamiguchi, *J. Cell Biol.* **188**, 429 (2010).
- [16] C. Pohl and Z. Bao, *Dev. Cell* **19**, 402 (2010).
- [17] H. Noji, R. Yasuda, M. Yoshida, and K. Kinoshita, Jr., *Nature (London)* **386**, 299 (1997).
- [18] P. Lenz, J.F. Joanny, F. Jülicher, and J. Prost, *Phys. Rev. Lett.* **91**, 108104 (2003).
- [19] N. Uchida and R. Golestanian, *Phys. Rev. Lett.* **104**, 178103 (2010).
- [20] I.R. Gibbons, *J. Cell Biol.* **91**, 107s (1981).
- [21] D. Bray, *Cell Movements* (Garland Publishing, New York, 2001), 2nd ed.
- [22] R. Di Leonardo, D. Dell'Arciprete, L. Angelani, and V. Iebba, *Phys. Rev. Lett.* **106**, 038101 (2011).
- [23] Y. Wu, B.G. Hosu, and H.C. Berg, *Proc. Natl. Acad. Sci. U.S.A.* **108**, 4147 (2011).
- [24] R.A. Simha and S. Ramaswamy, *Phys. Rev. Lett.* **89**, 058101 (2002).
- [25] T.B. Liverpool and M.C. Marchetti, *Phys. Rev. Lett.* **90**, 138102 (2003).
- [26] I.S. Aranson and L.S. Tsimring, *Phys. Rev. E* **67**, 021305 (2003).
- [27] Y. Hatwalne, S. Ramaswamy, M. Rao, and R.A. Simha, *Phys. Rev. Lett.* **92**, 118101 (2004).
- [28] K. Kruse, J.F. Joanny, F. Jülicher, J. Prost, and K. Sekimoto, *Phys. Rev. Lett.* **92**, 078101 (2004).
- [29] K. Kruse, J.F. Joanny, F. Jülicher, J. Prost, and K. Sekimoto, *Eur. Phys. J. E* **16**, 5 (2005).
- [30] J.L. Ericksen, *Arch. Ration. Mech. Anal.* **4**, 231 (1959).
- [31] F.M. Leslie, *Q. J. Mech. Appl. Math.* **19**, 357 (1966).
- [32] P.C. Martin, O. Parodi, and P.S. Pershan, *Phys. Rev. A* **6**, 2401 (1972).
- [33] P.G. de Gennes and J. Prost, *The Physics of Liquid Crystals* (Oxford University Press, Oxford, 1995), Vol. 2.
- [34] H. Stark and T.C. Lubensky, *Phys. Rev. E* **67**, 061709 (2003).
- [35] H. Stark and T.C. Lubensky, *Phys. Rev. E* **72**, 051714 (2005).
- [36] R. Voituriez, J.F. Joanny, and J. Prost, *Phys. Rev. Lett.* **96**, 028102 (2006).
- [37] G. Salbreux, J. Prost, and J.F. Joanny, *Phys. Rev. Lett.* **103**, 058102 (2009).
- [38] J.S. Bois, F. Jülicher, and S.W. Grill, *Phys. Rev. Lett.* **106**, 028103 (2011).
- [39] L. Giomi, L. Mahadevan, B. Chakraborty, and M.F. Hagan, *Phys. Rev. Lett.* **106**, 218101 (2011).
- [40] J. Elgeti, M.E. Cates, and D. Marenduzzo, *Soft Matter* **7**, 3177 (2011).
- [41] S. Fürthauer, M. Neef, S.W. Grill, K. Kruse, and F. Jülicher, *New J. Phys.* **14**, 023001 (2012).
- [42] L. Bocquet, W. Losert, D. Schalk, T.C. Lubensky, and J.P. Gollub, *Phys. Rev. E* **65**, 011307 (2001).
- [43] I.S. Aranson and L.S. Tsimring, *Rev. Mod. Phys.* **78**, 641 (2006).
- [44] S. Fürthauer, M. Strepel, S.W. Grill, and F. Jülicher, *Eur. Phys. J. E* **35**, 89 (2012).
- [45] J.C. Tsai, F. Ye, J. Rodriguez, J.P. Gollub, and T.C. Lubensky, *Phys. Rev. Lett.* **94**, 214301 (2005).
- [46] Note that  $\xi_t$  and  $\xi_\Omega$  are effective coefficients of the 2D theory that can be determined starting from the 3D description and depend on boundary conditions on the surfaces. In general, Eq. (11) might also have additional contribution of the form  $(p_i h_z)|_0^h$  and  $(p_z h_i)|_0^h$ . We do not write these contribution here for simplicity.
- [47] J.J. Essner, J.D. Amack, M.K. Nyholm, E.B. Harris, and H.J. Yost, *Development (Cambridge, U.K.)* **132**, 1247 (2005).
- [48] Y. Okada, S. Takeda, Y. Tanaka, J.C. Izpisua-Belmonte, and N. Hirokawa, *Cell* **121**, 633 (2005).
- [49] A.J.S. Klar, *Genetics* **165**, 269 (2003).